DIGITAL ELEVATION MODELING VIA CURVATURE INTERPOLATION FOR LIDAR DATA

HWAMOG KIM, JEFFREY L. WILLERS, SEONGJAI KIM

ABSTRACT. Digital elevation model (DEM) is a three-dimensional (3D) representation of a terrain's surface – for a planet (including Earth), moon, or asteroid – created from point cloud data which measure terrain elevation. Its modeling requires surface reconstruction for the scattered data, which is an ill-posed problem and most computational algorithms become overly expensive as the number of sample points increases. This article studies an effective partial differential equation (PDE)-based algorithm, called the *curvature interpolation method* (CIM). The new method iteratively utilizes curvature information, estimated from an intermediate surface, to construct a *reliable* image surface that contains all of the data points. The CIM is applied for DEM for point cloud data acquired by light detection and ranging (LiDAR) technology. It converges to a piecewise smooth image, requiring $\mathcal{O}(N)$ operations independently of the number of sample points, where N is the number of grid points.

1. INTRODUCTION

Point clouds are gained by scanning *three-dimensional* (3D) objects using various measuring techniques. The point cloud represents the set of points, each of which is defined by (x, y, z) coordinates. Point clouds are used for many purposes, including 3D *computer-aided design* (CAD) modeling for manufactured parts (reverse engineering), meteorology/quality inspection, visualization, animation, mass customization applications, and geosciences [11, 24]. In applications, point clouds are usually converted to polygon mesh or triangle mesh models, NURBS surface models, or CAD models through a process commonly referred to as *surface reconstruction*.

There are many techniques for surface reconstruction. Some approaches build a network of triangles over the existing vertices of the point cloud (Delaunay triangulation, marching triangles [12], and ball-pivoting [3]), while other approaches convert the point cloud into a volumetric distance field and reconstruct the implicit surface through a marching cubes algorithm [13]. However, in practice, the most

---

cited are polynomial interpolation such as nearest-neighbor, linear, and cubic methods [16, 23] due to their simplicity; these methods are easy to implement, but offer only low-quality results. Inverse-distance methods [21] are also used, although they are computationally expensive and become impractical as the number of samples increases. Another common interpolation model for point cloud data is the method of thin-plate splines, which is based on radial basis functions [22]; the method is hard to be practical due to a high computational complexity. See [7, 10] for efforts for the reduction of computational complexity of the method. In *light detection and ranging* (LiDAR) data processing, a frequently-used interpolation algorithm is the *inverse-distance weighting* (IDW) method [21].

Surface (image) reconstruction from point cloud (arbitrarily sampled) data is a challenging problem particularly when no constraint is imposed on their locations. The problem is ill-posed, first of all, and numerical methods solving its optimization formulation become overly expensive as the number of sample points increases [1, 2]. Furthermore, it is often the case that the constructed image is not an interpolator but an approximator, i.e., the reconstructed surface may not include all the data values.

In this article, the authors are interested in a novel PDE-based method called the *curvature interpolation method* (CIM), for surface reconstruction of terrain elevation data acquired by LiDAR technology. The new method utilizes a curvature information which is estimated from an intermediate surface of the point cloud data and plays a role of driving force for the construction of a reliable image surface. It is often the case that the constructed image surface does not contain all of the data values due to the estimated curvature. However, the misfit can be corrected by a recursive application of the CIM. The CIM is first studied for image zooming by one of the authors; see [5] and [15]. It has been verified that the CIM shows a *minimum* oscillatory behavior, and yet it results in piecewise smooth images containing all the data values.

The article is organized as follows. The next section briefly reviews the CIM and its recursive application, as preliminaries. Section 3 presents our digital elevation modeling strategies including an effective method for the reduction of Moiré effect inheritent in LiDAR data. Section 4 gives a set of numerical experiments, showing effectiveness of the suggested algorithm. At the end of this section, we summarize and conclude our experiments.

2. Preliminaries

This section presents a brief review for the curvature interpolation method (CIM) studied for image zooming [5, 15].

2.1. Curvature interpolation method (CIM).
Image zooming is a processing task to enlarge images by applying interpolation methods. The CIM was a PDE-based model; it begins with a selection of a curvature-related term which is to be estimated from the low resolution (LR) image, interpolated to the high resolution (HR) image grid, and incorporated as a driving force for the construction of HR image. PDE-based models that employ the (mean) curvature itself as the smoothing operator (e.g., the total variation (TV) model [20]) are known to have a tendency to converge to a piecewise constant image [6, 17]. Such a phenomenon is called *staircasing*. Thus the curvature would better be replaced by a more effective and

convenient operator $\mathcal{K}$. In [15], the authors adopted the following *gradient-weighted* (GW) curvature

$$\mathcal{K}(u) = -|\nabla u| \nabla \cdot \Big(\frac{\nabla u}{|\nabla u|} \Big). \tag{2.1}$$

Let Ω and $\widetilde{\Omega}$ be the original LR image domain and its α-times magnified HR image domain, $\alpha > 1$, respectively. Let $\widehat{\Omega}^0$ denote the set of pixel points in $\widetilde{\Omega}$ which can be expressed as $\alpha\mathbf{p}$, where $\mathbf{p}$ is a pixel point in Ω. Then the CIM [15] can be outlined as follows.

(I) Compute the GW curvature of the given LR image v^0:

$$\mathcal{K} = \mathcal{K}(v^0) \quad \text{on } \Omega. \tag{2.2}$$

(II) Interpolate $\mathcal{K}$ to obtain $\widehat{\mathcal{K}}$ on $\widetilde{\Omega}$.

(III) Solve, for u on $\widetilde{\Omega}$, the following constrained problem

$$\mathcal{K}(u) = \frac{1}{\alpha^2} \widehat{\mathcal{K}} \quad u|_{\widehat{\Omega}^0} = v^0. \tag{2.3}$$

In the above algorithm, the GW curvature measured from the LR image is interpolated and incorporated as an explicit driving force for the same GW curvature model on $\widetilde{\Omega}$. The driving force would help the model construct the HR image more effectively, enforcing the resulting image to satisfy the given curvature profile.

However, because the involved interpolation operations, the constructed surface (the solution of (2.3)) may have image values different from those in the corresponding LR grid points. A natural remedy for this drawback is to update image values iteratively by utilizing the difference between the LR image and the last updated image in the LR grid (misfit).

2.2. CIM with iterative refinement. When the CIM is applied for image zooming as in §2.1, the curvature of the LR image is first computed and then interpolated for an approximation of the curvature of the HR image. Such an approximated curvature shows a reasonable accuracy so that the CIM in each iteration can produce a reliable correction term to update the image surface. In image zooming, the given image may be viewed as an LR approximation of the target HR image. However, the case is quite different for the surface reconstruction for point cloud data, because the data loci are nonuniform and it is hard to estimate the curvature. Thus we first have to introduce an efficient scheme to estimate the surface and its curvature. As a strategy, we will construct an *intermediate surface*, from which useful curvature information would be obtained.

Let Ω be the image domain and Ω^0 the set of data pixels where image values are initialized as v^0. Our new surface reconstruction algorithm to be presented below involves three major steps: the construction of an intermediate surface, the curvature evaluation and smoothing, and surface reconstruction. When the reconstructed surface does not contain all of the prescribed image values (v^0), the difference can be corrected by applying the procedure iteratively. The following outlines our reconstruction algorithm.

> Initialize $\mathbf{u}_0 = 0$, on the image domain Ω
> Select the tolerance $\tau > 0$
> For $k = 1, 2, \cdots$

(i) Compute the misfit on Ω^0:

$$\mathbf{r}_{k-1} = \mathbf{v}^0 - \mathbf{u}_{k-1}$$

(ii) If $\|\mathbf{r}_{k-1}\| < \tau$, stop

(iii) Construct an intermediate surface ϕ_k:

$$-\Delta\phi_k = 0, \quad \mathbf{x} \in \Omega \setminus \Omega^0$$
$$\phi_k = \mathbf{r}_{k-1}, \quad \mathbf{x} \in \Omega^0 \qquad\qquad (2.4)$$
$$\nabla\phi_k \cdot \mathbf{n} = 0, \quad \mathbf{x} \in \partial\Omega$$

(iv) Evaluate A_k and K_k from ϕ_k:

$$K_k = A_k\boldsymbol{\phi}_k \approx \mathcal{K}(\phi_k)$$

(v) Smoothen K_k to get $\widetilde{K}_k$

(vi) Construct the correction surface $\mathbf{w}_k$:

$$A_k\mathbf{w}_k = \widetilde{K}_k$$

(vii) Update:

$$\mathbf{u}_k = \mathbf{u}_{k-1} + \mathbf{w}_k$$

Here $\mathbf{v}^0$ is the vector representation of the sampled data v^0, $\mathbf{r}_{k-1}$ denotes the misfit defined on the sample points Ω^0, ϕ_k is an intermediate surface, a solution of an interior point value problem of the Laplace equation, $\mathbf{n}$ denotes the unit outward normal defined on the image boundary $\partial\Omega$, and $\|\cdot\|$ is either L^2 norm or the maximum norm. The equation $\nabla\phi_k \cdot \mathbf{n} = 0$ is called the no-flux boundary condition. The interior point value problem in (2.4)(iii) is incorporated for the construction of an intermediate surface, due to its simplicity. See [9] for effective computational methods including finite difference schemes, a smoothing strategy, and algebraic solvers.

In this article, we apply (2.4) for digital elevation modeling for LiDAR point cloud data; we call the algorithm the *CIM with iterative refinement* (IR-CIM).

3. Digital Elevation Modeling

3.1. **LiDAR data acquisition.** For the previous decade or so, the *light detection and ranging* (LiDAR) technology has grown in popularity, meeting the need and replacing conventional surveying techniques which are time-consuming and labor-intensive [8, 14, 18, 19]. LiDAR data are acquired in a form of point cloud; helicopter or fixed-wing LiDAR systems scan the surface below the aircraft, collecting reflected light signals in a scan rate of 50,000 to 100,000 pulses per second, achieving high accuracies up to 5cm, for most cases. Due to their high resolution and rich information content, LiDAR data are utilized for a wide range of applications with different requirements in terms of resolution, accuracy, and surface representation. Applications include digital elevation model (DEM) topography, flood risk mapping, watershed analysis, coastal erosion analysis, landslides, tree canopy analysis, transmission line mapping, and urban applications [4]. LiDAR is an active remote sensing technique, analogous to radar, but using laser light.

See Figure 1, which depicts a schematic illustration of LiDAR data acquisition, along with the aircraft trajectory and the LiDAR scan coverage for a field survey over Mississippi farms near Mississippi State University (MSU), May 12, 2011. LiDAR instruments built on an aircraft measure the round-trip time for a pulse
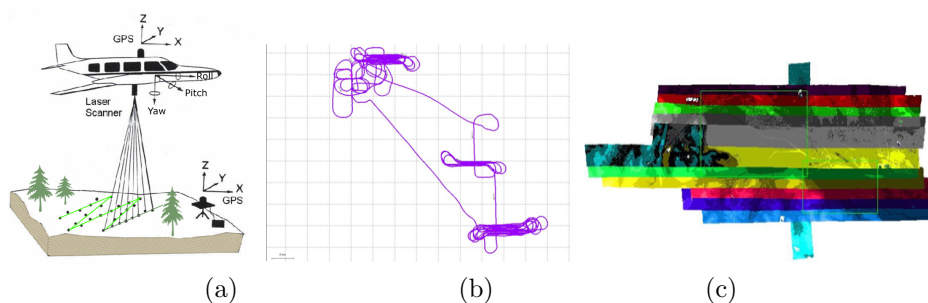
(a) (b) (c)

FIGURE 1. LiDAR data acquisition: (a) a schematic illustration of data collection, (b) the aircraft trajectory for a field survey over Mississippi farms near Mississippi State University, May 12, 2011, and (c) one of the LiDAR scan coverages.

of laser energy to travel between the sensor and a target. This incident pulse of energy (usually with a near-infrared wavelength for vegetation studies) reflects off of canopy (branches, leaves) and ground surfaces and back to the instrument where it is collected by a telescope. The travel time of the pulse, from initiation until it returns to the sensor, provides a distance or range from the instrument to the object. The acquired information is then transformed, with the aid of a minimum of four GPS satellites, to obtain a 3D position fix. The individual data points are collected to form a set of point cloud data. As one can see from Figure 1(c), the data are collected with the scan strips overlapped, in order to densely cover the scan area by cloud points.
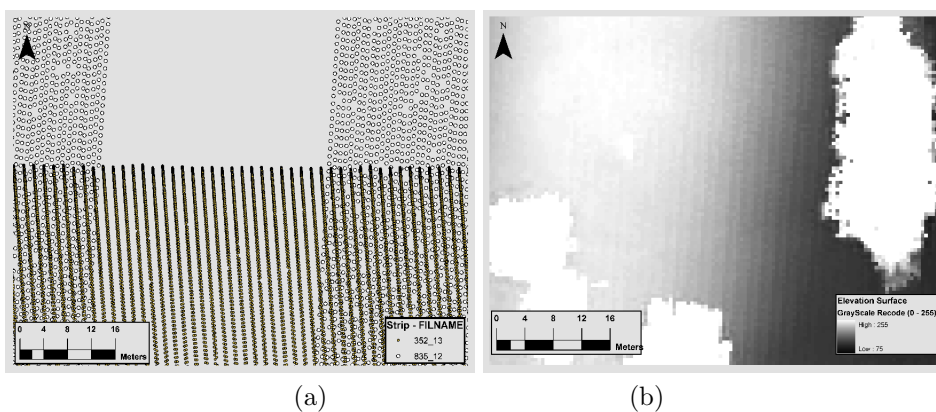

(a) (b)

FIGURE 2. LiDAR soil survey over Mississippi farms near MSU: (a) a missing gap in the point cloud data and (b) the elevation surface processed by the IDW built in ArcMap.

3.2. **Moiré patterns.** DEMs derived from LiDAR techniques are growing in popularity as a tool for use in soil survey, in particular. This form of remotely sensed

elevation data can serve multiple purposes, not the least of which is the visual interpretation of landforms and soil parent materials.

However, as one can see from Figure 2(a), the data may involve missing gaps; for which it is necessary to either perform extra rounds of data acquisition or incorporate a very effective interpolation algorithm for the reconstruction of reliable elevation surfaces. Figure 2(b) depicts a elevation surface processed by the inverse-distance weighting (IDW) method built in ArcMap. (ArcMap is one of state-of-the-art geospatial processing programs.) In the figure, white regions are related to trees and buildings and the ground elevation decreases in the SE direction. The parallel features running in the SSW-NNE direction are processing artifacts involved during the surface reconstruction of the data which have been acquired through scan lines in the same direction with multiple overlapped scan strips. Thus the parallel features are kinds of Moiré interference patterns. Contours and topographic parameters (gradients, curvatures) derived from such elevation surfaces *must* include a noisy pattern; for most applications, they have been further processed (filtered, smoothed), often manually, to make them suitable [19].

3.3. **Correction strategy for Moiré effect.** As aforementioned, it is a common practice in LiDAR data acquisition that the data are collected with the scan strips overlapped. However, due to various technical reasons, data sets obtained from different scans covering the same overlapped area may have misfits in elevation values. When these data sets are used without an appropriate correction, the resulting surface may involve serious artifacts including oscillatory patterns.
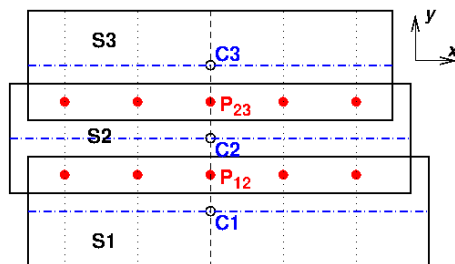

FIGURE 3. A schematic illustration of LiDAR scan coverages. The dash-dot lines (in blue) indicate the center of the scan strips and the red bullets in the overlapped areas are check points.

The elevation misfits can be eliminated using local elevation averages that are obtained from each of the data sets and measured over the overlapped scan areas. For a simple presentation, we first assume that the scan coverages overlap maximum twice as shown in Figure 3. In the figure, S_i, $i = 1, 2, 3$, denote the scan strips, the dash-dot lines (in blue) indicate the center of the scan strips, and C_i are points on the center lines. The check points P_{12} and P_{23} represent centroids of overlapped areas between the scans S_1 and S_2 and between S_2 and S_3, respectively. The data correction begins with partitioning the overlapped areas and setting check points, the two rows of red points shown in Figure 3. Then the average elevation values on each of overlapped scan strips are computed in a vicinity of the check points, using the data values at pixels that are scanned and assigned from both sides of the adjacent scan strips. If the average elevations obtained from the two different scan

strips are different at the check points, the data on the two adjacent strips can be adjusted *piecewise linearly* so that the resulting data sets have the same average elevations at the check points.
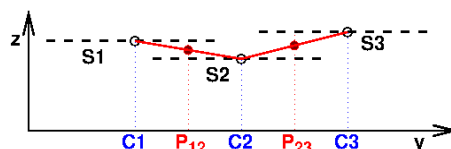

FIGURE 4. A schematic illustration for data correction through local elevation averages.

In Figure 4, we assume that the average elevation at P_{12} computed from S_1 (E_{12}) is larger than that from S_2 (E_{21}). Then the data elevation values in S_1 and S_2 can be corrected by adjusting the data values on half-strips linearly. For example, assuming that $\overrightarrow{C_1C_2}$ is parallel to the y-axis, the elevation values can be adjusted as follows.

$$(x, y, z) \in S_1 \mapsto (x, y, z'),$$
$$(x, y, z) \in S_2 \mapsto (x, y, z''),$$

(3.1)

where

$$z' = z + \frac{(E_{21} - E_{12})/2}{p_{12,y} - c_{1,y}}\,(y - c_{1,y}),$$

$$z'' = z + \frac{(E_{21} - E_{12})/2}{c_{2,y} - p_{12,y}}\,(c_{2,y} - y).$$

Here $c_{1,y}$, $c_{2,y}$, $p_{12,y}$ are the second coordinates of C_1, C_2, P_{12}, respectively. Note that when $y = p_{12,y}$,

$$z' = z + (E_{21} - E_{12})/2, \quad z'' = z + (E_{21} - E_{12})/2;$$

the corrections have the same magnitude from the both sides.

The algorithm for the elimination of Moiré patterns should also incorporate the following concerns.

• *Array of check points*: The misfits, the differences of the average elevations on overlapped areas, may differ when measured from different regions. Thus we have introduced a line of check points in each of overlapped areas, aligned parallel to the x direction, as shown in Figures 3. The Moire effects can be reduced effectively by applying piecewise bilinear functions, as explained earlier in this subsection.

• *Multiple overlaps*: The scan coverages may overlap more than twice for some regions; in practice, it is often the case that some regions are covered three times. In this case, the array of check points should include more rows in the cross direction of the scan flight (the y direction), in order to represent the misfits more appropriately. For example, let the data overlap m times in the scan strip S_k. Then the misfit correction function (MCF) for the data in S_k can be defined to be a polynomial of degree at most $m - 1$ in the y direction. The MCF is still piecewise linear in the x direction.

• *Accuracy of MCFs*: It is occasionally the case that data loci are distributed with a largely varying density; the data may involve missing gaps. Thus, local elevation averages obtained from raw data may not accurately represent the real elevation

averages for some regions and therefore the MCFs can be erroneous. In order to overcome the difficulty, we may consider the following strategy.

(i) Construct the surfaces for each of the scan strips using the IR-CIM (2.4).
(ii) Compute the local elevation averages using the elevation values from the reconstructed surfaces.
(iii) Construct MCFs for each of overlapped strips.
(iv) Apply the MCFs to the reconstructed surfaces.
(v) Blend the corrected surfaces for a single surface covering the whole scan area.
(vi) Improve the blended surface by applying the IR-CIM.

The final step is not expensive computationally, because the blended surface would be a good approximation of the final result.

4. Numerical experiments

This section gives numerical examples to show effectiveness of the IR-CIM and the Moiré-pattern reduction algorithm applied for DEM modeling. The 12 strips of LiDAR point cloud data acquired over Mississippi farms near Mississippi State University, as shown in Figure 1(c), are utilized for the modeling. The data set includes approximately 37 million points counted including multiple arrivals.
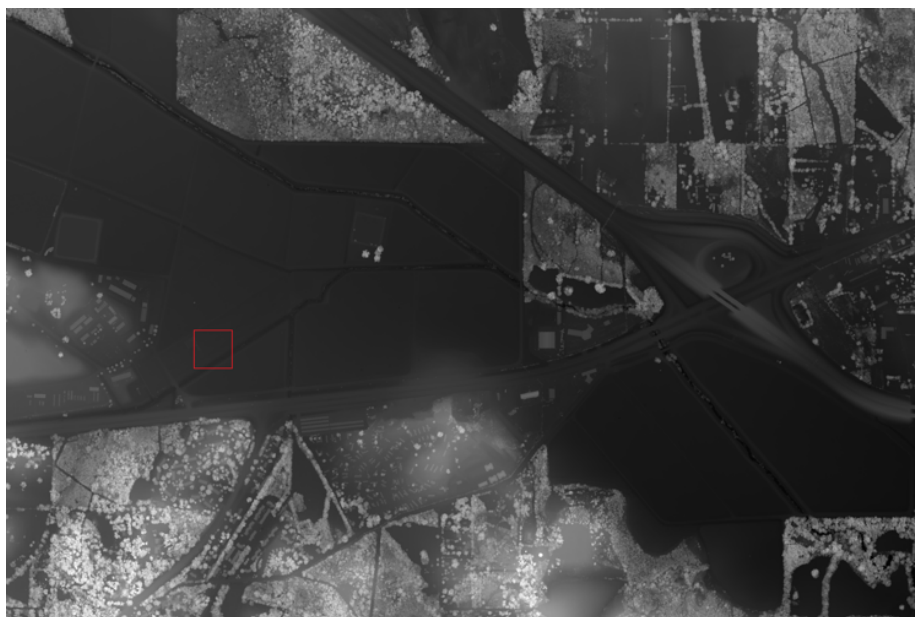

Figure 5. Final image surface in 96 million pixels, covering a region of 3km×2km square with a quarter-meter resolution.

Figure 5 depicts the final elevation image in 96 million pixels, which covers a region of 3Km×2Km square with a quarter-meter resolution. In this study, the Moiré effect is reduced using the elevation averages measured from the data, applying the formulas in (3.1). About 17% of the pixel values of the image can be assigned directly from the elevation values in the data and other pixel values are

computed using the IR-CIM (2.4). The algorithm (written in a combination of C
and C++) converges in 3 iterations, taking 67.2 seconds on a desktop computer for
the whole processing.
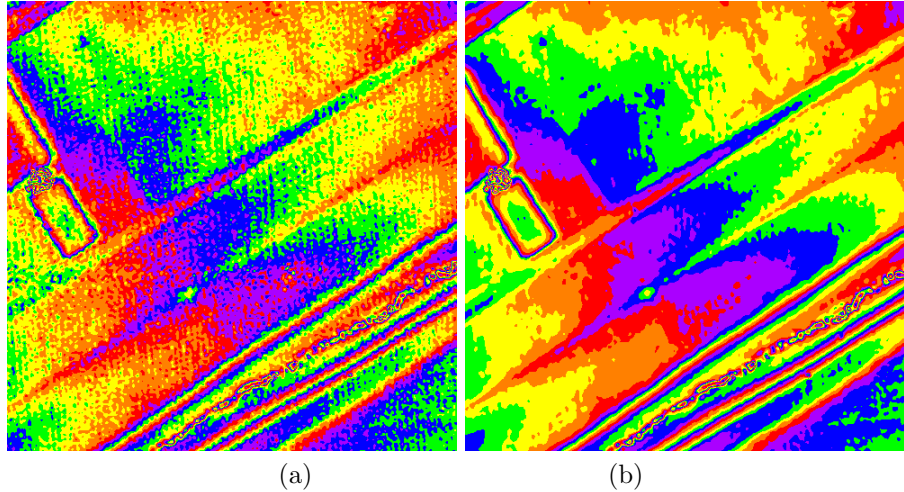

(a)   (b)

FIGURE 6. Moiré effect and its correction.

Figure 6 shows image surfaces, shown in a prism view of 1cm resolution in
elevation, covering the region marked with a square (in red) in Figure 5. When the
data values are used without correction of Moiré effect, the reconstructed surface
involves oscillatory patterns as in Figure 6(a). On the other hand, our Moiré-effect
reduction algorithm has eliminated the oscillatory patterns effectively as depicted
in Figure 6(b). In the last image, Moiré effect is hardly observable even shown in
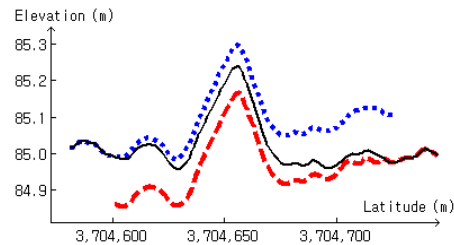1cm resolution in elevation.

FIGURE 7. Correction of elevation values, shown on a vertical line
segment. The solid curve (in black) represents the corrected eleva-
tion values over an overlapped region of two scan strips.

To further investigate effectiveness of the suggested algorithm, we select a vertical
segment in the mid of the square-marked region in Figure 5 and compare elevation
values. In Figure 7, the dotted and dashed curves indicate elevation values obtained
from separate scan strips of an overlapped region, while the solid curve (in black)
represents the corrected elevation values over the overlapped region of the two scan
strips. As one can see from the figure, the elevation values are corrected using a

locally linear correction function effectively, to result in a continuous and reliable image surface.

Conclusions. Surface reconstruction from point cloud data is a challenging problem particularly when no constraint is imposed on their locations, as for LiDAR data. This article has applied an effective PDE-based algorithm, called the curvature interpolation method (CIM), for a set of LiDAR data acquired from a field survey over Mississippi farms near Mississippi State University. For the reduction of oscillatory patterns appearing over overlapped regions of scan strips, we have introduced an effective misfit correction function (MCF) which is piecewise linear. A recursive application of the CIM with the suggested MCF has converged in 3-4 iterations to produce reliable and piecewise smooth image surfaces that introduce no Moiré effect, taking less than a second per million pixels on common desktop computers.

References

[1] M. Arigovindan, M. Sühling, P. Hunziker, M. Unser; *Variational image reconstruction from arbitrarily spaced samples: A fast multiresolution spline solution*, IEEE Trans. Image Process., 14 (2005), pp. 450–460.

[2] R. Beatson, W. A. Light, S. Billings; *Fast solutions of radial basis function interpolation equations: Domain decomposistion methods*, SIAM J. Sci. Comput., 22 (2000), pp. 1717–1740.

[3] F. Bernardini, J. Mittleman, H. Rushmeier, C. Silva, G. Taubin; *The ball-pivoting algorithm for surface reconstruction*, IEEE Transactions on Visualization and Computer Graphics, 5 (1999), pp. 349–359.

[4] T. Cary; *New research reveals current and future trends in LiDAR applications*, Industry Insights, (2009), pp. 8–9.

[5] Y. Cha, G. Y. Lee, S. Kim; *Image zooming by curvature interpolation and iterative refinement*, SIAM J. Imaging Sciences, 7 (2014), pp. 1284–1308.

[6] T. Chan, J. Shen; *Image Processing and Analysis*, SIAM, Philadelphia, 2005.

[7] F. Chen, D. Suter; *Using fast multipole method for accelerating the evaluation of splines*, IEEE Comput. Sci. Eng., 5 (1998), pp. 24–31.

[8] Y.-W. Choi, Y.-W. Jang, H.-J. Lee, G.-S. Cho; *Three-dimensional LiDAR data classifying to extract road point in urban area*, IEEE Geoscience and Remote Sensing Letters, 5 (2008), pp. 725–729.

[9] W. Cordell, H. Kim, J. Willers, S. Kim; *Image reconstruction for arbitrarily spaced data using curvature interpolation*, in Proceedings of The 2013 International Conference on Image Processing, Computer Vision, and Pattern Recognition, 2013, pp. 506–512.

[10] A. Faul and M. Powel; *Proof of convergence of an iterative technique for thin plate spline interpolation in two dimensions*, Adv. Comput. Math., 11 (1999), pp. 183–192.

[11] A. Glassner; *Principles of Digital Image Synthesis*, Morgan Kaufmann, San Mateo, CA, 1995.

[12] A. Hilton, A. J. Stoddart, J. Illingworth, T. Wandeatt; *Marching triangles: Range image fusion for complex object modeling*, in Proceedings of International Conference on Image Processing, vol. 1, 1996, pp. 381–384.

[13] H. Hoppe, T. DeRose, T. Duchamp, J. McDonald, W. Stuetzle; *Surface reconstruction from unorganized points*, in SIGGRAPH'92: Proceedings of the 19th Annual Conference on Computer Graphics and Interactive Techniques, New York, NY, USA, 1992, ACM, pp. 71–78.

[14] F. Hosoi, Y. Nakai, K. Omasa; *Estimation and error analysis of woody canopy leaf area density profiles using 3-D airborne and ground-based scanning Lidar remote-sensing techniques*, IEEE Trans. on Geoscience and Remote Sensing, 48 (2010), pp. 2215–2223.

[15] H. Kim, Y. Cha, S. Kim; *Curvature interpolation method for image zooming*, IEEE Trans. Image Process., 20 (2011), pp. 1895–1903.

[16] T. Lehmann, C. Gönner, K. Spitzer; *Survey: Interpolation methods in medical image processing*, IEEE Trans. Medical Imaging, 18 (1999), pp. 1049–1075.

[17] A. Marquina, S. Osher; *Explicit algorithms for a new time dependent model based on level set motion for nonlinear deblurring and noise removal*, SIAM J. Sci. Comput., 22 (2000), pp. 387–405.

[18] J. McKinion, J. Willers, J. Jenkins; *Comparing high density LIDAR and medium resolution GPS generated elevation data for predicting yield stability*, Computers and Electronics in Agriculture, 74 (2010), pp. 244–249.

[19] H. Mitasova, L. Mitas, R. S. Harmon; *Simultaneous spline approximation and topographic analysis for Lidar elevation data in open-source GIS*, IEEE Geoscience and Remote Sensing Letters, 2 (2005), pp. 375–379.

[20] L. Rudin, S. Osher, E. Fatemi; *Nonlinear total variation based noise removal algorithms*, Physica D, 60 (1992), pp. 259–268.

[21] D. Shepard; *A two-dimensional interpolation function for irregularly-spaced data*, in Proceedings of the 1968 ACM National Conference, 1968, pp. 517–524.

[22] G. Turk J. OB́rien; *Shape transformation using variational implicit functions*, in Proc. ACM SIGGRAPH, Los Angeles, CA, 1999, pp. 335–342.

[23] K. Turkowski; *Filters for common resampling tasks*, in Graphics Gems I, A. S. Glassner, ed., Academic Press Professional, Inc., San Diego, CA, USA, 1990, pp. 147–165.

[24] D. Watson; *Contouring: A Guide to the Analysis and Display of Spatial Data*, Pergamon, New York, 1992.

Hwamog Kim
Department of Mathematics and Statistics, Mississippi State University,
Mississippi State, MS 39762, USA
   E-mail address: hk404@msstate.edu

Jeffrey L. Willers
USDA-ARS, Genetics and Precision Agriculture Research,
Mississippi State, MS 39762, USA
   E-mail address: jeffrey.willers@ars.usda.gov

Seongjai Kim
Department of Mathematics and Statistics, Mississippi State University,
Mississippi State, MS 39762, USA
   E-mail address: skim@math.msstate.edu